Canada 9

AIRCRAFT FLOW EFFECTS ON CLOUD DROPLET IMAGES AND CONCENTRATIONS

by

A.M. Drummond

National Aeronautical Establishment

AERONAUTICAL NOTE
NAE-AN-21
NRC NO. 23543

85-3236/

NATIONAL AERONAUTICAL ESTABLISHMENT

SCIENTIFIC AND TECHNICAL PUBLICATIONS

AERONAUTICAL REPORTS:

Aeronautical Reports (LR): Scientific and technical information pertaining to aeronautics considered important, complete, and a lasting contribution to existing knowledge.

Mechanical Engineering Reports (MS): Scientific and technical information pertaining to investigations outside aeronautics considered important, complete, and a lasting contribution to existing knowledge.

AERONAUTICAL NOTES (AN): Information less broad in scope but nevertheless of importance as a contribution to existing knowledge.

LABORATORY TECHNICAL REPORTS (LTR): Information receiving limited distribution because of preliminary data, security classification, proprietary, or other reasons.

Details on the availability of these publications may be obtained from:

Publications Section,
National Research Council Canada,
National Aeronautical Establishment,
Bldg. M-16, Room 204,
Montreal Road,
Ottawa, Ontario
K1A 0R6

ÉTABLISSEMENT AÉRONAUTIQUE NATIONAL

PUBLICATIONS SCIENTIFIQUES ET TECHNIQUES

RAPPORTS D'AÉRONAUTIQUE

Rapports d'aéronautique (LR): Informations scientifiques et techniques touchant l'aéronautique jugées importantes, complètes et durables en termes de contribution aux connaissances actuelles.

Rapports de génie mécanique (MS): Informations scientifiques et techniques sur la recherche externe à l'aéronautique jugées importantes, complètes et durables en termes de contribution aux connaissances actuelles.

CAHIERS D'AÉRONAUTIQUE (AN): Informations de moindre portée mais importantes en termes d'accroissement des connaissances.

RAPPORTS TECHNIQUES DE LABORATOIRE (LTR): Informations peu disséminées pour des raisons d'usage secret, de droit de propriété ou autres ou parce qu'elles constituent des données préliminaires.

Les publications ci-dessus peuvent être obtenues à l'adresse suivante:

Section des publications
Conseil national de recherches Canada
Établissement aéronautique national
Im. M-16, pièce 204
Chemin de Montréal
Ottawa (Ontario)
K1A 0R6

UNLIMITED
UNCLASSIFIED

AIRCRAFT FLOW EFFECTS ON CLOUD DROPLET IMAGES AND CONCENTRATIONS

LES EFFETS D'ÉCOULEMENT D'AIR AUTOUR D'UNE AVION SUR LES IMAGES ET LES CONCENTRATIONS MESURÉES DE GOUTTELETTES DANS LES NUAGES

by/par

A.M. Drummond

National Aeronautical Establishment

OTTAWA
JUNE 1984

AERONAUTICAL NOTE
NAE-AN-21
NRC NO. 23508

S.R.M. Sinclair, Head/Chef
Flight Research Laboratory/
Laboratoire de recherche en vol

G.M. Lindberg
Director/Directeur

SUMMARY

Cloud physics measurements by the Twin Otter aircraft are affected to some degree by local flow effects from the wing and from the probe canister. Droplet images and concentration are distorted in the worst case by no more than 20% for an aircraft lift coefficient (C_L) of 0.75 and by only a few percent for low values of C_L. Corrections for a Particle Measuring Systems probe mounted on a short pylon at the inboard spanwise location have been given which are based on an experimentally verified model for the flow velocity.

SOMMAIRE

Quelques données physiques des nuages mesurées par l'avion "Twin Otter" sont modifiées, à un certain degré, par les effets d'écoulement d'air local autour de l'aile et de la boîte contenant la sonde. Les images et les concentrations mesurées des gouttelettes sont déformées au plus de 20% pour un coefficient de portance (C_L) de 0.75 et de quelques pour-cent pour les petites valeurs du C_L.

Les corrections qui sont présentées pour les données ont été obtenues avec la sonde "Particle Measuring System" montée sur un pylôn court fixé à un point interne de l'aile, ces corrections furent dérivées d'un modèle pour la vitesse de l'écoulement et vérifiées expérimentalement.

CONTENTS

		Page
	SUMMARY	(iii)
	SYMBOLS	(v)
1.0	INTRODUCTION	1
2.0	EQUATIONS OF MOTION	1
	2.1 Initial Position	5
	2.2 Final Position	5
3.0	THE LOCAL FLOW VELOCITIES	5
4.0	CLOUD PHYSICS IMPLICATIONS	6
5.0	RESULTS FOR VELOCITY	7
6.0	RESULTS FOR TRAJECTORY EXPANSION	8
7.0	CORRECTIONS TO CLOUD PHYSICS MEASUREMENTS	9
8.0	CONCLUSIONS	10
9.0	REFERENCES	10
10.0	ACKNOWLEDGEMENT	10

TABLES

Table		Page
1	Values of C as a Function of R_e	11
2	Atmospheric Properties	12
3	Dimensions and Location of Sample Volume	12
4	Aircraft Lift Coefficient for Speed and Altitude	13

ILLUSTRATIONS

Figure		Page
1	Twin Otter Cloud Physics Research Aircraft	15
2	Starboard Probes on Two Pylons	16
3	Co-ordinate System	17

ILLUSTRATIONS (Cont'd)

Figure		Page
4	Velocity at Probe	18
5	Velocity at Probe	19
6	Velocity at Probe	20
7	Velocity at Probe	21
8	Velocity at Probe	22
9	Drop Velocity	23
10	Velocity Ratio Parameters	24
11	Trajectory Expansion	25
12	Trajectory Expansion	26
13	Trajectory Expansion	27
14	Trajectory Expansion	28
15	Trajectory Expansion	29
16	Expansion Ratio Parameters	30

SYMBOLS

Symbol	Definition
A	intercept of straight line
a	fundamental length — quarter chord
B	slope of straight line
C_D, C_{D_s}	drag coefficient in high R_e, Stokes flow
$C(R_e)$	C_D / C_{D_s}
C_L	lift coefficient
c	speed of sound, ft/sec
D, D_s	drag in high, low (Stokes) Reynolds Number flow
ER	expansion ratio

SYMBOLS (Cont'd)

Symbol	Definition
g	acceleration due to gravity
h	altitude
K_1, K_2	constants
L	aircraft lift
m	mass
P	air static pressure, mb
R_e	Reynolds Number
S	wing area
t	time
t*	a/V
T	air temperature, °R
U, W	drop velocity in x′, z′ axes
U_a, W_a	air velocity in x′, z′ axes
$\bar{u}_a$, w_a	non-dimensional air velocity due to wing alone in x, z axes
u, w	non-dimensional drop velocity in x, z axes
u_a, w_a	total non-dimensional air velocity in x, z axes
V	air velocity at infinity
VR	velocity ratio
x′, z′	co-ordinates in wing plane
x, z	non-dimensional co-ordinates in wing plane
x_s	distance ahead of sphere center
α	angle of attack
δ	drop diameter
τ	t/t*
ρ, ρ_d	density of air, drop

SYMBOLS (Cont'd)

Symbol	Definition
μ, ν	absolute, kinematic viscosity of air
ϵ/a	wing thickness parameter
η	complex co-ordinate in wing plane
ζ	complex co-ordinate in cylinder plane
Sub SL	sea level

AIRCRAFT FLOW EFFECTS ON CLOUD DROPLET IMAGES AND CONCENTRATIONS

1.0 INTRODUCTION

The Twin Otter aircraft has been instrumented as a cloud physics research aircraft (Ref. 1) and has been used for a number of years in co-operation with the Atmospheric Environment Service. The aircraft can measure atmospheric state variables and air motion in real time. In addition, cloud droplets and particles can be sized and imaged by Particle Measuring Systems (PMS) probes that are mounted under the wings. It was known that the measurements by the probes could be influenced by the flow around the wings and by the cylindrical body (canister) which houses the working components of the probe. The aircraft and PMS probes are shown in Figures 1 and 2.

A theoretical model of local flow velocity at the sampling point of a PMS probe has been developed (Ref. 2) and experimentally verified by flight measurements using a pitot-static equipped PMS canister mounted under the Twin Otter wing at four different positions. This model will be used in assessing local flow effects. It is felt that meaningful conclusions on cloud physics measurements can be made as a result of this experimental verification.

This report discusses implications of local flow effects on cloud physics measurements related to droplets. Results for non-spherical particles cannot be accurately calculated because such particles can be widely variable in shape and can have an unpredictable angular orientation while passing through the probe sample volume. Further, the density of ice particles or snowflakes can vary from 0.2 gms/cc (say) to about 1 gm/cc. The motion of a particle is determined by its drag-to-mass ratio; hence, variations in mass and aerodynamic properties of non-spherical particles make accurate calculations of their motion impossible.

In the sections that follow, an analysis of aircraft-induced errors in cloud physics measurements will be made for water drops. We will first develop the equations of motion for the drop, pose the boundary value problem for drops being sampled, solve the problem numerically and present results for drop velocity and trajectory expansion at one probe location. A method to correct cloud physics results obtained from the Twin Otter will be presented.

2.0 EQUATIONS OF MOTION

The co-ordinate system (Fig. 3) is fixed to the mid-chord point of the aircraft wing, x' and z' being orthogonal. The x' axis is the line joining the leading and trailing edges of the wing and it is positive towards the trailing edge. This axis is inclined at an angle α to the flow at infinity. The z' axis is positive up. The droplet has velocity components U, W in the x', z' directions and the local flow velocity has components U_a, W_a with respect to these axes. The equations of motion for the drop in the x', z' axes are

$$m\frac{dU}{dt} = -D_{x'}$$

$$m\frac{dW}{dt} = -D_{z'} - mg \qquad (1)$$

The motion of the drop is considered to be two-dimensional, the spanwise positional variation being neglected in the present case. For probe locations near the wing tip, this restriction would not be applicable. The flow about the Twin Otter wing is virtually two-dimensional at the present PMS probe spanwise mounting locations (0.618 and 0.747 of semispan).

The x′ and z′ components of the drag are written in terms of the droplet velocity with respect to the air in the form:

$$D_{x'} = D \frac{(U - U_a)}{\sqrt{(U - U_a)^2 + (W - W_a)^2}}$$

$$D_{z'} = D \frac{(W - W_a)}{\sqrt{(U - U_a)^2 + (W - W_a)^2}} \qquad (2)$$

Following Reed (Ref. 3), the drag (D) is written in terms of the drag in Stokes flow (D_s).

$$D = D(D_s/D_s)$$

$$= (C_D/C_{D_s})3\pi\mu\delta\sqrt{(U - U_a)^2 + (W - W_a)^2} \qquad (3)$$

where C_D/C_{D_s} is a function of the Reynolds Number and δ is the drop diameter. The absolute air viscosity is μ. The Reynolds Number is

$$R_e = (\delta/\nu)\sqrt{(U - U_a)^2 + (W - W_a)^2} \qquad (4)$$

where ν is the air kinematic viscosity.

Substituting (3) and (2) in (1) and writing the drop mass in terms of drop diameter and density (ρ_d) leads to:

$$\frac{dU}{dt} = -\left(\frac{C_D}{C_{D_s}}\right)\frac{18}{\delta^2}\frac{\rho}{\rho_d}\nu(U - U_a) \qquad (5)$$

$$\frac{dW}{dt} = -g - \left(\frac{C_D}{C_{D_s}}\right)\frac{18}{\delta^2}\frac{\rho}{\rho_d}\nu(W - W_a) \qquad (6)$$

Equations (5) and (6) are best handled in a non-dimensional form where velocities are measured relative to the air velocity at infinity (V), lengths are measured relative to the quarter-chord length of the wing (a) and a non-dimensional time τ is defined:

$$\begin{aligned} u &= U/V \\ w &= W/V \\ x &= x'/a \\ z &= z'/a \\ \tau &= t/t^* \\ t^* &= a/V \end{aligned} \tag{7}$$

Substitution of (7) in (5) and (6) leads to

$$\frac{dx}{d\tau} = u \tag{8}$$

$$\frac{dz}{d\tau} = w \tag{9}$$

$$\frac{du}{d\tau} = - C(R_e)\, K_1\, (u - u_a) \tag{10}$$

$$\frac{dw}{d\tau} = - C(R_e)\, K_1\, (w - w_a) - K_2 \tag{11}$$

where the following non-dimensional quantities have been defined:

$$C(R_e) = C_D / C_{D_s} \tag{12}$$

$$K_1 = \frac{18}{(\delta/a)^2} \frac{\rho}{\rho_d} \frac{\nu}{Va} \tag{13}$$

$$K_2 = ga/V^2 \tag{14}$$

$$R_e = \frac{Va}{\nu} (\delta/a) \sqrt{(u - u_a)^2 + (w - w_a)^2} \tag{15}$$

The constants K_1 and K_2 group the aerodynamic and gravitational parameters respectively. The data from References 3 and 5 for values of C are given in Table 1 for various values of R_e.

Equations (8) to (11) are nonlinear ordinary differential equations for the drop co-ordinates x and z. The local flow velocities u_a and w_a are not functions of time in steady flight. They describe the spatial variation of the local flow effects from the wing and PMS probe canister. Solutions to the above system must be performed numerically because of the variation of C with R_e and the variation of u_a and w_a with x and z.

The initial values of the droplet velocity components are

$$u(0) = \cos\alpha$$
$$w(0) = \sin\alpha \qquad (16)$$

The initial position of the droplet must be chosen such that its final position is within the probe sample volume. Thus, the boundary value problem is posed:

> find the initial position of the drop with a given initial velocity such that the final position condition is satisfied at an unspecified velocity.

The trajectory from initial to final position is obtained by numerically integrating Equations (8) to (11) using the data from Reed and Vennard (Table 1) to interpolate for C and a Runge-Kutta-Gill integration routine with variable step size. The standard atmosphere is assumed (Ref. 4, p. 21) where temperature, density and static pressure are determined by altitude h relative to the sea level (SL) values:

$$T = T_{SL} - 3.566 * (h/1000) \qquad (17)$$

$$c = c_{SL} * \sqrt{T/T_{SL}} \qquad (18)$$

$$\rho = \rho_{SL} \exp(-0.0297 * h/1000) \qquad (19)$$

$$P = P_{SL} \exp(-0.0347 * h/1000) \qquad (20)$$

The variation of kinematic viscosity with altitude is obtained to a very close approximation by linear interpolation between the entries in Table 2. This table also contains the sea level values of the variables in Equations (17) to (20).

The boundary value problem is solved by a "shooting method" where the initial position of the drop is chosen and the final position is calculated. If this final position is not sufficiently close to the desired final position, then the initial position is chosen again and the procedure is repeated. A simple algorithm for choosing the initial position was developed by trial and error that required only two iterations for large drops and no more than six for small drops in order to converge to a solution of the boundary value problem.

2.1 Initial Position

As stated before, the initial position of the drop must be found so that its final position is within a specified distance of the top/bottom of the sample volume. The initial x co-ordinate of the drop was taken to be 31 quarter-chords upstream. The initial z co-ordinate was varied to solve the boundary value problem. The initial x was chosen to be far enough away from the wing so that the flow effects due to the wing were negligible. To prove this, one set of calculations with an initial x of -21 was computed and the results showed no discernible difference from those obtained using an initial x of -31. Similar conclusions were drawn when an initial x of -41 was used. All the results presented here used an initial x of -31.

2.2 Final Position

A successful solution to the boundary value problem occurs when the final position of the droplet is "sufficiently" close to the desired value. In this work, a computational box in the x, z plane was placed around the final point. The dimensions of the box relative to the central, final point were $\pm$ 0.01 quarter-chords in the x direction, and $\pm\ 3\delta/a$ or $\pm\ 2 \times 10^{-4}$, which ever was bigger, in the z direction.

All of the computations were performed for the case of a PMS 2D-C probe mounted on the short pylon at the inboard location along the span. The dimensions and sample volume location are given in Table 3. The probe counts droplets that are within its depth of field. Hence, both the top and bottom of the sample volume had to be considered as final positions for the drops.

3.0 THE LOCAL FLOW VELOCITIES

The local flow velocities u_a and w_a are functions of position. These velocities were calculated by modeling the flow about the Twin Otter wing using Joukowski aerofoil therory (Ref. 2) and including canister effects. The validity of the model was established by measuring the flow velocity at the four locations where probes are carried under the Twin Otter wings.

A brief summary of the results of Reference 2 is included. The Twin Otter wing was taken to have a rectangular planform, a symmetrical section of 16% thickness, an elliptical spanwise load distribution and no twist. The simplest Joukowski transformation was employed which caused the model of the real wing to have a cusped trailing edge instead of having the correct trailing edge angle. The forward half of the wing section was well represented as a Joukowski aerofoil.

The main conclusion of that report was that the Joukowski aerofoil theory (including canister effects) could be used to obtain u_a and w_a anywhere ahead of the wing quarter-chord point with an accuracy better than 97%, for the probe location of Table 3, in the range of aircraft lift coefficients (C_L) applicable to cloud penetrations. The lift coefficient is:

$$C_L = L/(1/2\ \rho V^2 S)$$

For straight and level flight, the lift L equals the aircraft weight.

A point in the wing plane is located by the complex co-ordinate η

$$\eta = x + iz \qquad (21)$$

and the corresponding complex co-ordinate ζ in the cylinder plane is located by the conformal transformation

$$\zeta = (\eta/2) \pm \sqrt{(\eta/2)^2 - 1} \tag{22}$$

The sign is chosen so that ζ is outside the cylinder. The velocity in the wing plane is calculated most easily by the relation:

$$\bar{u}_a - iw_a = \left[\exp(-i\alpha) - \frac{(1+\epsilon/a)^2}{(\zeta+\epsilon/a)^2} \exp(i\alpha) + 2i \frac{(1+\epsilon/a)}{(\zeta+\epsilon/a)} \sin(\alpha) \right] \times \left(\frac{\zeta^2}{\zeta^2 - 1} \right) \tag{23}$$

where the overbar on the x component of velocity signifies that only flow due to the wing is described by Equation (23).

The thickness parameter is ϵ and the wing angle of attack is α. A method of obtaining ϵ for a given wing thickness is described in Reference 2.

The effects of the canister were included in a simple, approximate fashion. The discussion in Reference 2 on the modeling of the flow ahead of the hemispherical end of the canister can be summarized. The flow due to the wing in the x direction, $\bar{u}_a$, is modified by the flow about a sphere. The following relation is used for the final estimate of the local velocity u_a because the canister is considered to be "small" and imbedded in the flow about the wing:

$$u_a = \bar{u}_a \left(1 - (r_s/x_s)^3\right)$$

where r_s is the radius of the spherical end of the canister and x_s is the distance of the drop from the center of the sphere. The small effects of the sphere on w_a are neglected and $\bar{u}_a$ is taken to be along the axis of the canister. Both r_s and x_s are in terms of the fundamental length 'a'.

4.0 CLOUD PHYSICS IMPLICATIONS

There are two main implications of aircraft-induced flow effects on cloud physics results. The first is that the images of drops formed by PMS probes are distorted unless the drops pass through the probe sample volume at the true airspeed of the aircraft. The scanning rate of the laser in the PMS probe is adjusted to give the correct images to drops under the assumption that they are moving at the aircraft speed and not at a different speed because of local flow effects. For example, if the drop velocity is 80% of aircraft true airspeed as it passes through an imaging probe, then its dimension in the x direction will be distorted by the ratio of five to four relative to the spanwise dimension. The drop will appear elongated in the x direction.

Since the velocity of a drop that passed through the bottom of the sample area is in general different from the velocity of one of the same size that passed through the top, then some rule must be developed for chosing the corrective factor to be applied to images. Both drops will be in focus and will be imaged but there is no way to tell which image goes with a "top drop" or a "bottom drop". It is suggested that the average of the velocities be used. Acceptable accuracy is possible only if the "top" and "bottom" velocities are not too different.

The second effect is that measurements of drop concentrations (number per unit volume) are distorted because drops of different sizes as counted by the probes originate from cloud volumes of different sizes and different locations. It is usually assumed that drops move on straight lines so that the volume swept out by a probe is determined only by the frontal dimensions of its sample area and the aircraft speed. However, small drops tend to follow the local flow streamlines and if the streamlines at infinity expand (or contract) relative to their spacing at the probe, then the volume used in the concentration calculation is incorrect. Large drops ignore local flows and pass through the probe sample area as though they had moved on straight lines (almost) that remain parallel. In this case, the assumed volume used in the concentration calculations is the correct one. Concentration measurements become a function of drop size because trajectories of different sized drops have different starting points.

5.0 RESULTS FOR VELOCITY

Drop trajectories that solved the boundary value problem were computed for one probe location. Trajectories passing through the top and bottom of the sample area were studied and the drop velocity as it passed through those positions was computed. At the same time, the ratio of the difference in the initial z co-ordinate to the difference in the final z co-ordinate of trajectories through the top and bottom of the sample areas was calculated. This calculation is pertinent to analysis of concentration errors while the former is related to image distortions.

The velocity ratio is

$$VR = \sqrt{u^2 + w^2}$$

If VR is less than one, then the droplet is moving slower than the aircraft speed.

Figures 4, 5 and 6 show three typical results for the droplet velocity ratio at the top and bottom of the sample area as a function of drop size. Each figure is applicable to one set of flight conditions (aircraft lift coefficient).

In all cases, the velocity ratio of the largest drop tends to one while the ratio for the smallest drop approaches that of the local airflow. Both of these results were expected. As aircraft lift coefficient increases, the velocity ratio for the small drops decreases and the local minimum for moderately sized drops becomes less pronounced. The minimum occurs at a smaller drop size for increasing C_L but it usually occurs for drop diameters between 40 and 80μ. The exact nature of the curve in this region depends on the integrated effects of the velocity field experienced by the drop as it approaches the probe.

The cause of the minimum in Figures 4 to 6 is the inertia of the drop. As the drop approaches the PMS probe, there is a decreasing magnitude of the velocity field due to the wing. The inertia of the droplet does not let it slow as quickly as the local flow. Then, the velocity field starts to accelerate and the drop lags this trend because of its inertia. Hence, it goes through the sample volume at a velocity less than that of the local flow. The above discussion is not true for drops so small that they essentially follow local flow, nor for drops so large that the local flow is of no consequence.

In all, nine values of C_L were chosen for computation of the velocity ratio at the top and bottom points of the probe sample volumes. The range of variables was V = 60, 70, 80 m/s and h = 6,000, 10,000 and 14,000 ft. and the aircraft weight was chosen as 10,000 lbs in all cases. The nine values of the corresponding C_L are shown in Table 4. Results for only three of these were shown in Figures 4 to 6 but they are typical of the other six.

For a constant drop size, the average velocity ratio can be plotted versus C_L for drops that pass through the sample volume. This procedure was adopted for a few drop sizes and the results are shown in Figures 7 and 8. Figure 8 applies to small drops and shows the minimum discussed above. A least-squares fit to the nine values was made and the straight line is the result of the procedure. Close examination of the figures reveals that the deviation of each point from the line is small, but that data at each speed really fall into separate populations. The aircraft C_L does not supply exact correlation to the data. The reason is that the local flow velocity is a linear function of C_L but the droplet drag depends on atmospheric viscosity as well. However, the correlation with lift coefficient is considered to be adequate.

Figure 9 is a plot of all the velocity ratios versus C_L and drop size for the average of the top and bottom velocities at the probe sample volume. This plot masks the slight variation of drop velocity with speed and altitude. The dotted line in the C_L-diameter plane shows where the straight lines for smaller drops would pierce the plane at high C_L. This figure shows how the local minimum moves to smaller drop sizes as C_L increases. The results are extrapolated to a large value of C_L (1.2). The local flow velocity model is not very reliable in this area because the wing is approaching a stalled condition.

Figure 10 shows the intercepts and slopes of the straight lines drawn in Figure 9. The smoothness of the curves show that interpolation between the data points is valid and that limited extrapolation to drops larger than 1 mm in diameter is permissible.

6.0 RESULTS FOR TRAJECTORY EXPANSION

The trajectory expansion ratio ER is defined as:

$$ER = \Delta z_i / \Delta z_f$$

where Δz is the positive difference in position between "top" and "bottom" trajectories previously described and the subscripts "i" and "f" refer to initial and final position respectively. If ER is less than one, there has been "expansion" from the initial to the final position.

Figures 11, 12, and 13 show the expansion ratio for the same values of C_L that applied to the previously described velocity ratio results (Figs. 4, 5 and 6). There is more scatter in the data because both the numerator and denominator in the expression for ER are obtained from the difference of two small numbers of the same order of magnitude. Also, a solution is accepted if a drop is within the computational box which admits a tolerance on x_f and z_f. However, the smoothness of the data is sufficient to allow the ER as shown in the figures to be used to correct cloud measurements. These results are restricted to the case of spherical drops.

At low C_L, Figure 11, there is almost no drop concentration distortion due to local flow effects because ER is very nearly equal to one for all drop sizes. As C_L increases, (Figs. 12 and 13) ER decreases for small drops and remains near one for large drops. Underestimation of drop concentrations is the general result.

The data from the above three figures can be plotted versus C_L for a given drop size (Figs. 14 and 15). Figure 15 applies to smaller drops. A least-squares straight line fit to the nine data points is shown. Very small deviations of data from the line are evident. The results are qualitatively the same as those for the velocity ratio but there are small quantitative differences. If desired, a plot similar to Figure 9 could be drawn to suit the expansion ratio.

Figure 16 shows the slopes and intercepts of the straight lines obtained in Figures 14 and 15 when plotted versus drop diameter. Again there is more scatter when compared to the similar plot of velocity ratio parameters (Fig. 10). The trends and shapes of the curves on Figure 16 are about the same as those on Figure 10.

7.0 CORRECTIONS TO CLOUD PHYSICS MEASUREMENTS

Drops passing through the sample volume at speeds other than the aircraft speed have images that are distorted. In general, the images of all drops will need correction. The drop dimension in the x direction must be multiplied by the velocity ratio appropriate to the drop diameter and aircraft lift coefficient. The diameter δ is obtained from the drop dimension perpendicular to the x, z plane, which is given by the photo-diode array. Sufficient data to compute aircraft C_L must be recorded at an adequately high sampling rate so that the x dimension of each drop can be scaled in the software at the C_L appropriate to the time of diameter measurement.

Let:

$$VR(\delta, C_L) = A(\delta) + B(\delta)\, C_L$$

where $A(\delta)$ and $B(\delta)$ are the slope and intercept of a straight line as illustrated in Figures 7 and 8. These two parameters are plotted in Figure 10. Interpolation functions could be determined empirically for $A(\delta)$ and $B(\delta)$ so that if one knew δ and C_L, the correct velocity ratio could be calculated. Conversely, the data of Figure 10 could be used to form a table of values for various values of δ. This table could be stored in the computer and used for on-board analysis or for later analysis on the ground. At each value of δ, interpolation between entries in the table would lead to an approximation to the correct values of A and B. The coarseness of the approximation would depend on the size of the interval between table entries. Perhaps the time available in the computation cycle would determine these intervals and this could dictate the accuracy of image correction caused by drop velocity effects.

Measurements of drop concentrations can be corrected in the same way by using $A(\delta)$ and $B(\delta)$ from Figure 16. Division of concentration data by the expansion ratio ER allows the effects of local flow to be accounted for. Without this correction, concentration data are under-estimated if ER is less than one and over-estimated if ER is greater than one. Small drops at low C_L exhibit the latter error while most drops experience the former error.

The numerical results of the calculations presented in this report apply to one PMS probe installation on the Twin Otter: the inboard spanwise position with the short pylon. These calculations can be repeated for the other three possible PMS mounting locations in order to obtain corrections to measurements at those locations. The purposes of this report have been fulfilled without doing these calculations. In any event, the computer programs and data reduction logic have been developed. The calculations could be routinely performed and would not show large differences from the results quoted here because the flow is not greatly different at those points.

In the range of C_L between 0.3 and 0.75, the concentration measurements of small drops are at most 18% under-estimated at present. The concentration measurements of large drops are approximately correct. The same is true for images, which are at worst distorted by only 20% in the axis ratio determination. These errors are not large but they can be nearly removed by applying the methods described here using Figures 10 and 16 to obtain the slope and intercept for each drop size. Application of these parameters to the measured aircraft lift coefficient should lead to image and concentration measurements correct to a few percent. The theoretical local flow velocity is more nearly equal to the measured value at two other probe locations (Ref. 2) so one would expect even better corrections for probes mounted here.

The use of C_L based on aircraft weight to correct cloud physics measurements can be criticized in so far as the local flow is not completely steady because of aircraft response to gusty air within a cloud. However, some of the in-flight measurements described in Reference 2 were taken under "gusty" conditions and the effect of this unsteady flow on the correlations presented there could not be noticed. It is stated without proof that unless the aircraft motion becomes very unsteady, the methods presented here will still apply.

Errors in imaging and concentration measurements can arise from many sources and only those resulting from aircraft flow effects have been discussed. It is beyond the scope of this report to attempt a general treatment of all types of errors.

8.0 CONCLUSIONS

Cloud physics measurements by the Twin Otter aircraft are affected to some degree by local flow effects from the wing and from the probe canister. Droplet images and concentrations are distorted in the worst case by no more than 20% for an aircraft lift coefficient of 0.75 and by only a few percent at lower values of C_L. Typically, cloud penetrations take place at a C_L of between 0.4 and 0.6. Corrections for a Particle Measuring Systems 2D-C probe mounted at the inboard location on the short pylon have been given which are based on an experimentally verified model for the local flow velocity.

9.0 REFERENCES

1. MacPherson, J.I.
Morgan, J.M.
Lum, K.
The NAE Twin Otter Atmospheric Research Aircraft.
NRC, Laboratory Technical Report, LTR-FR-80, National Research Council Canada, Ottawa, March 1981.

2. Drummond, A.M.
MacPherson, J.I.
Theoretical and Measured Airflow About the Twin Otter Wing.
NRC, Aeronautical Note, NAE AN-19, National Research Council Canada, Ottawa, March 1984.

3. Reed, W.H. the III
An Analytical Study of the Effect of Airplane Wake on the Lateral Dispersion of Aerial Sprays.
NACA Report 1196, 1954.

4. Dommasch, D.O.
Sherby, S.S.
Connolly, T.F.
Airplane Aerodynamics.
4th Edition, Pitman, 1967.

5. Vennard, J.K.
Elementary Fluid Mechanics.
3rd Edition, John Wiley & Sons, 1955.

10.0 ACKNOWLEDGEMENT

The efforts of Ian MacPherson of the Flight Research Laboratory in helping to bring this report to completion are gratefully acknowedged.

TABLE 1

VALUES OF C AS A FUNCTION OF R_e

R_e	C	R_e	C
0	1.00	20.0	2.291
0.05	1.009	25.0	2.489
0.1	1.018	30.0	2.673
0.2	1.037	35.0	2.851
0.4	1.073	40.0	3.013
0.6	1.103	50.0	3.327
0.8	1.142	60.0	3.60
1.0	1.176	80.0	4.11
1.2	1.201	100.0	4.59
1.4	1.225	120.0	5.01
1.6	1.248	140.0	5.40
1.8	1.267	160.0	5.76
2.0	1.285	180.0	6.16
2.5	1.332	200.0	6.52
3.0	1.374	250.0	7.38
3.5	1.412	300.0	8.26
4.0	1.447	350.0	9.00
5.0	1.513	400.0	9.82
6.0	1.572	500.0	11.46
8.0	1.678	1000.0	19.44
10.0	1.782	2227.0	37.2
12.0	1.901	3000.0	50.0
14.0	2.009	4000.0	66.7
16.0	2.109	5000.0	83.3
18.0	2.198	6000.0	100.0

From References 3 and 5.

TABLE 2

ATMOSPHERIC PROPERTIES

h ft	ν ft^2/sec	T°R	c ft/sec	ρ slugs/ft^3	P mb
Sea level (SL)	1.576×10^{-4}	518.69	1116.4	0.002377	1013.2
6000	1.869×10^{-4}				
14000	2.234×10^{-4}				

TABLE 3

DIMENSIONS AND LOCATION OF SAMPLE VOLUME

Sample volume co-ordinates (in quarter chords)

Position	x	z
Center	-1.595	-0.58
Top	-1.595	-0.518
Bottom	-1.595	-0.642
Canister nose center	-1.130	-0.58

Wing Chord: 78 inches
Probe: PMS 2D-C mounted at 61.8% of semi-span

TABLE 4

AIRCRAFT LIFT COEFFICIENT FOR SPEED AND ALTITUDE

Speed ms^{-1}	Altitude ft	C_L
80	6000	0.348
80	10000	0.392
80	14000	0.441
70	6000	0.454
70	10000	0.511
70	14000	0.576
60	6000	0.618
60	10000	0.696
60	14000	0.784

Weight = 10000 lbs

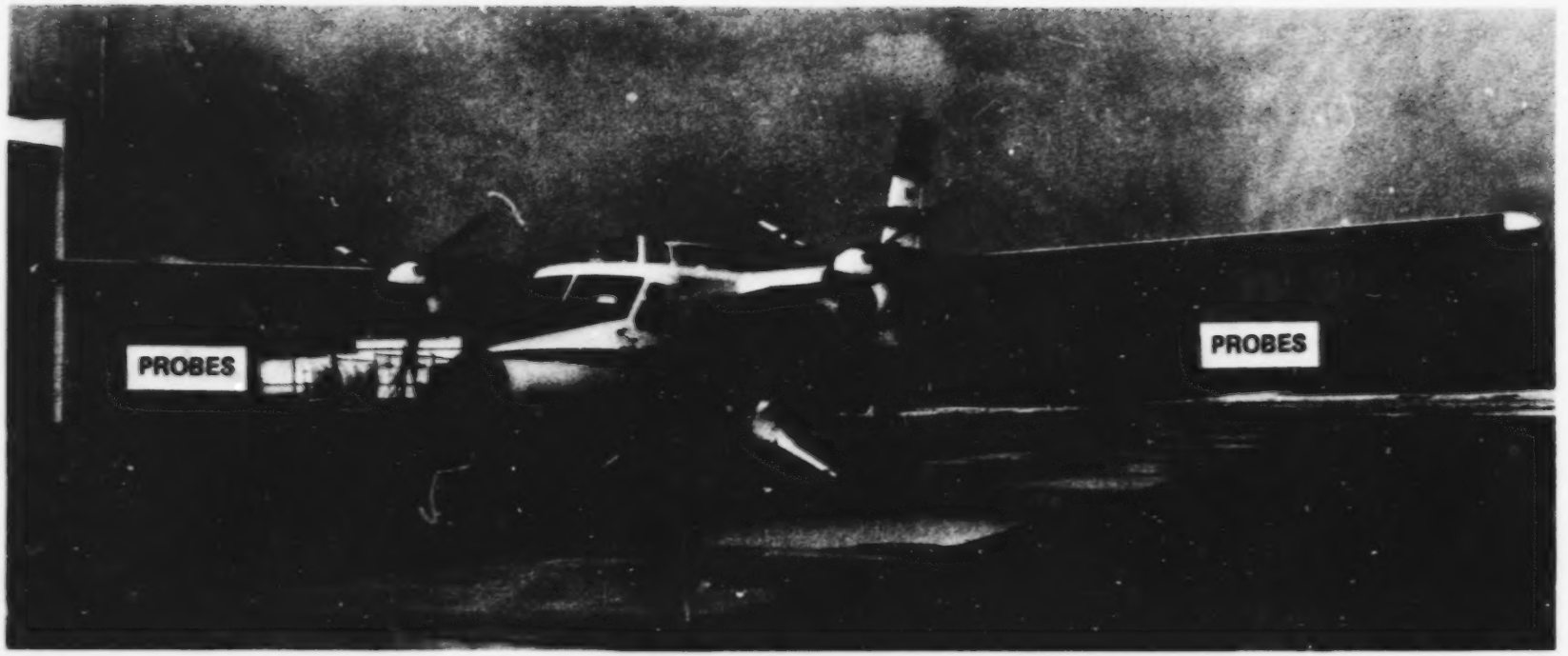

FIG. 1: TWIN OTTER CLOUD PHYSICS RESEARCH AIRCRAFT

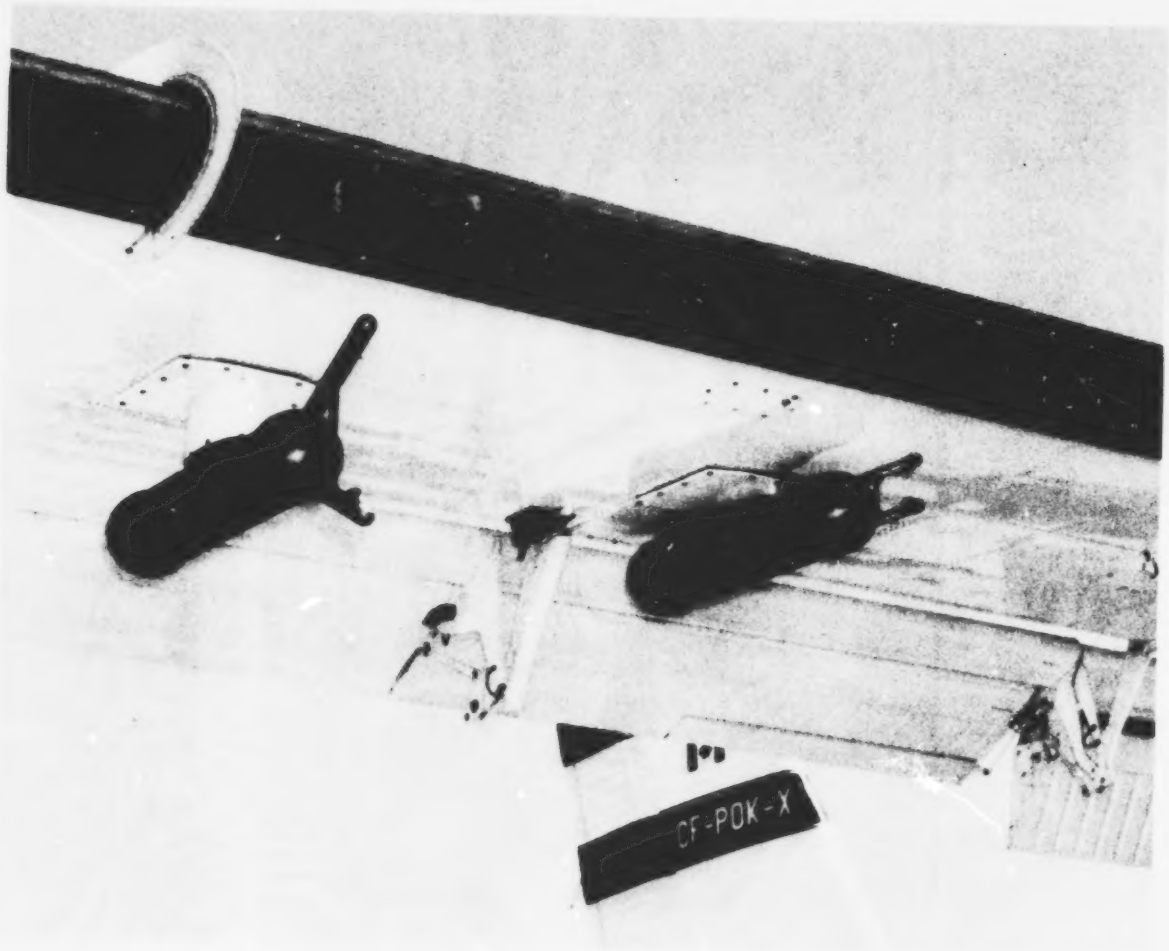

FIG. 2: STARBOARD PROBES ON TWO PYLONS

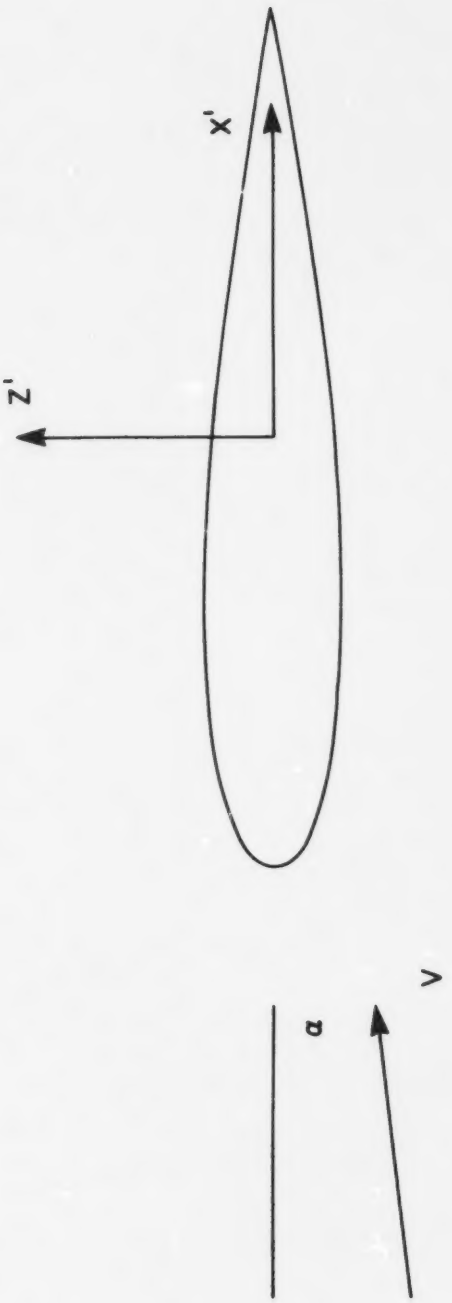

FIG. 3: CO-ORDINATE SYSTEM

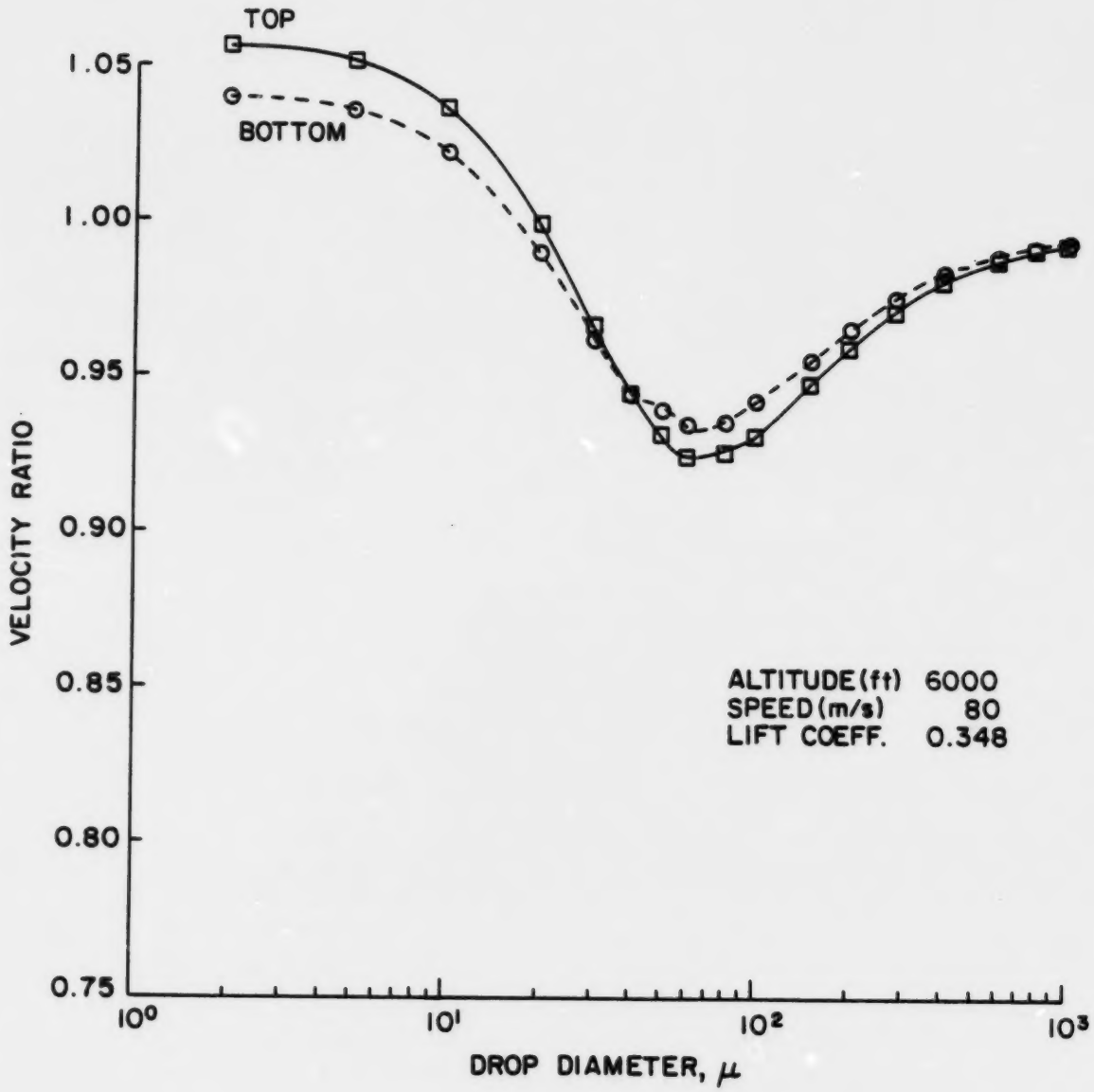

FIG. 4: VELOCITY AT PROBE

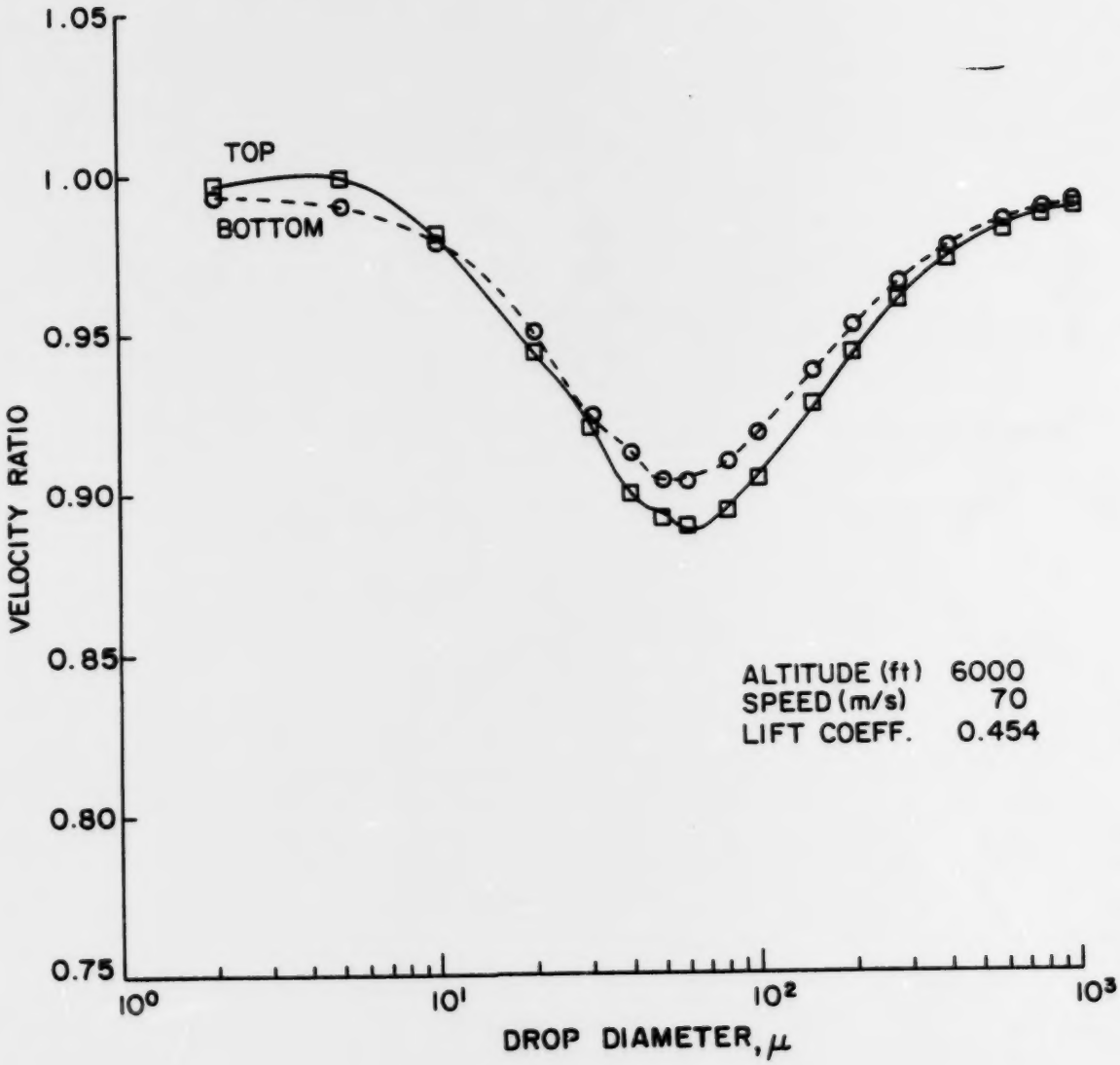

FIG. 5: VELOCITY AT PROBE

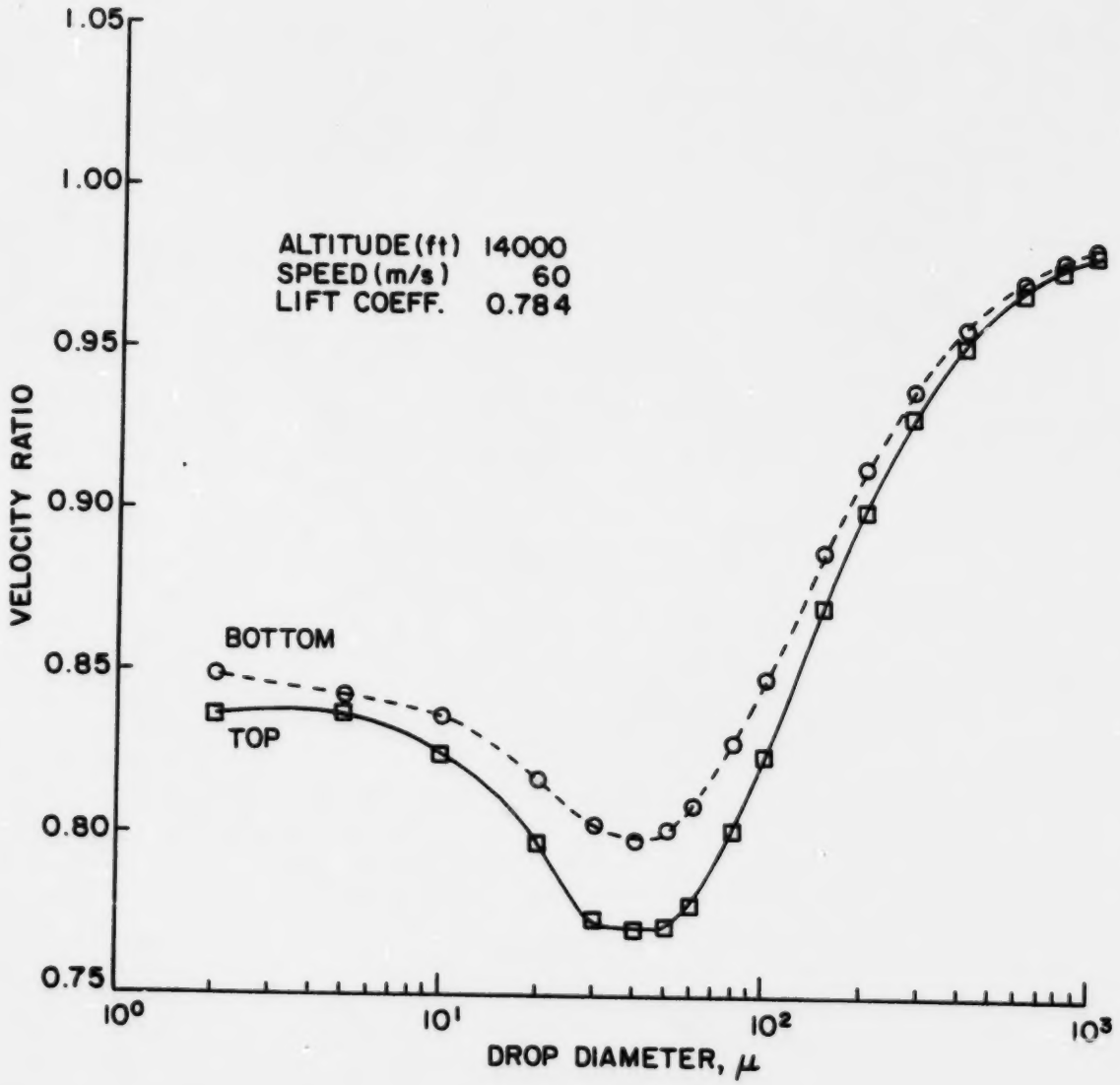

FIG. 6: VELOCITY AT PROBE

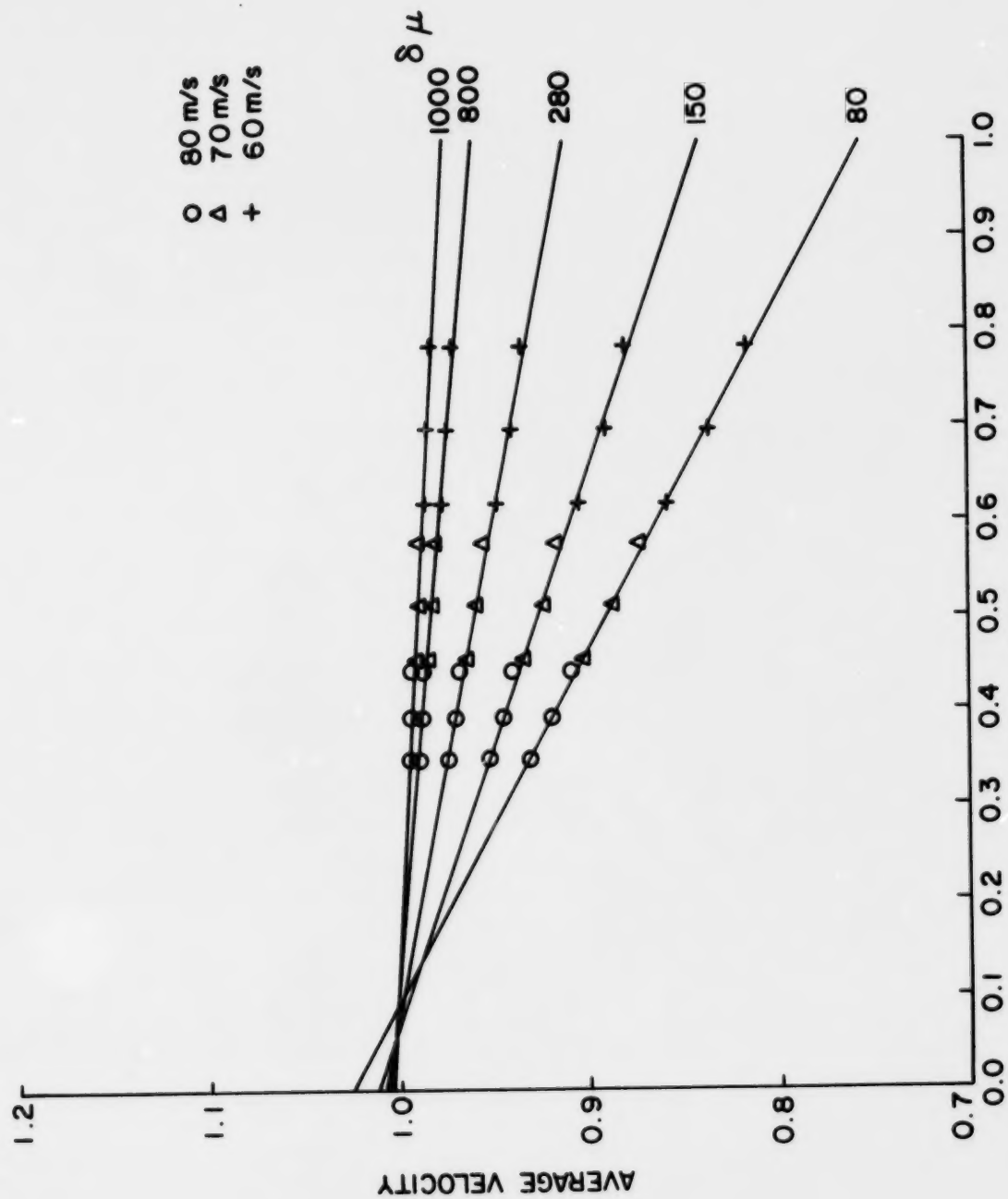

FIG. 7: VELOCITY AT PROBE

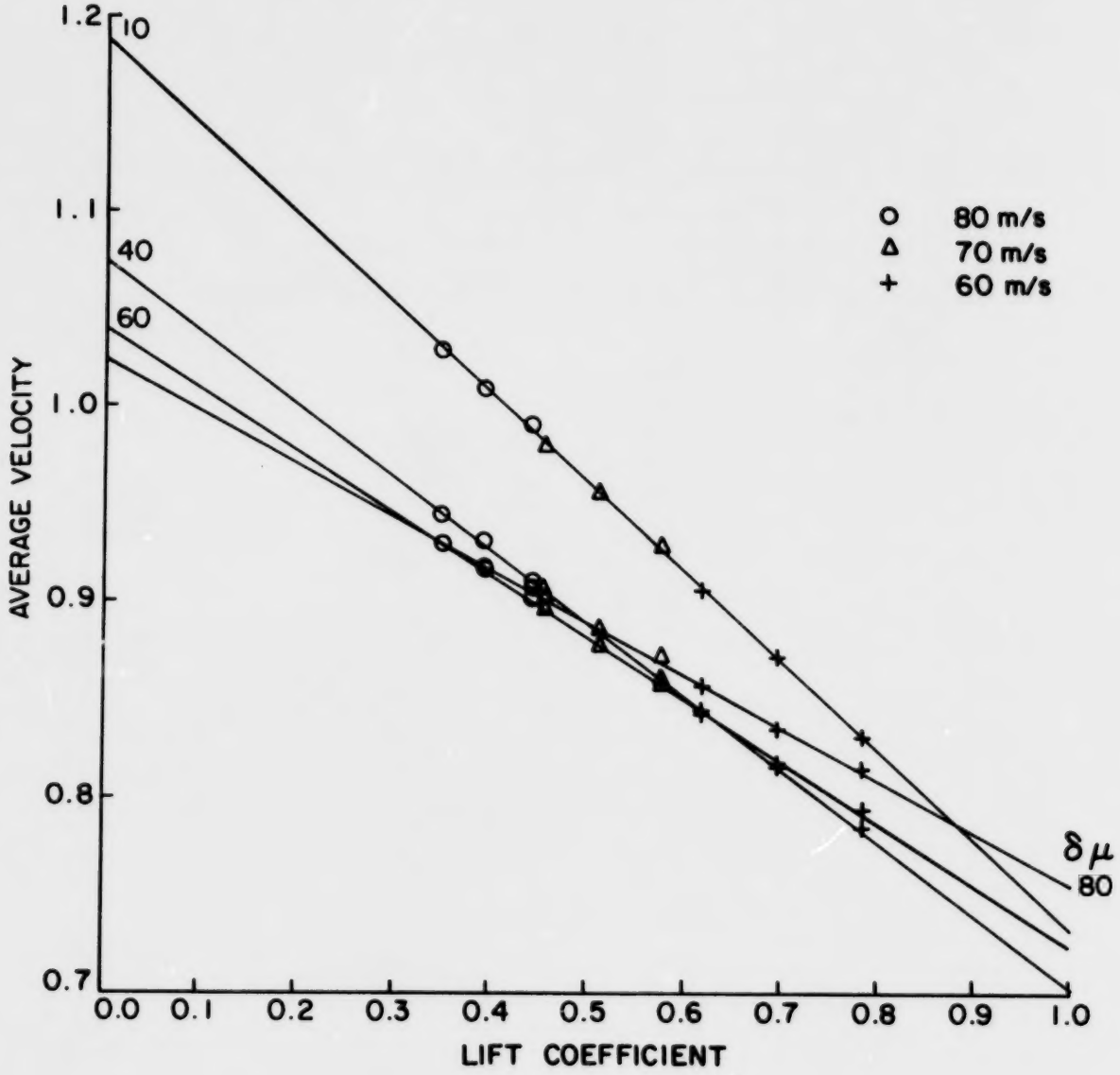

FIG. 8: VELOCITY AT PROBE

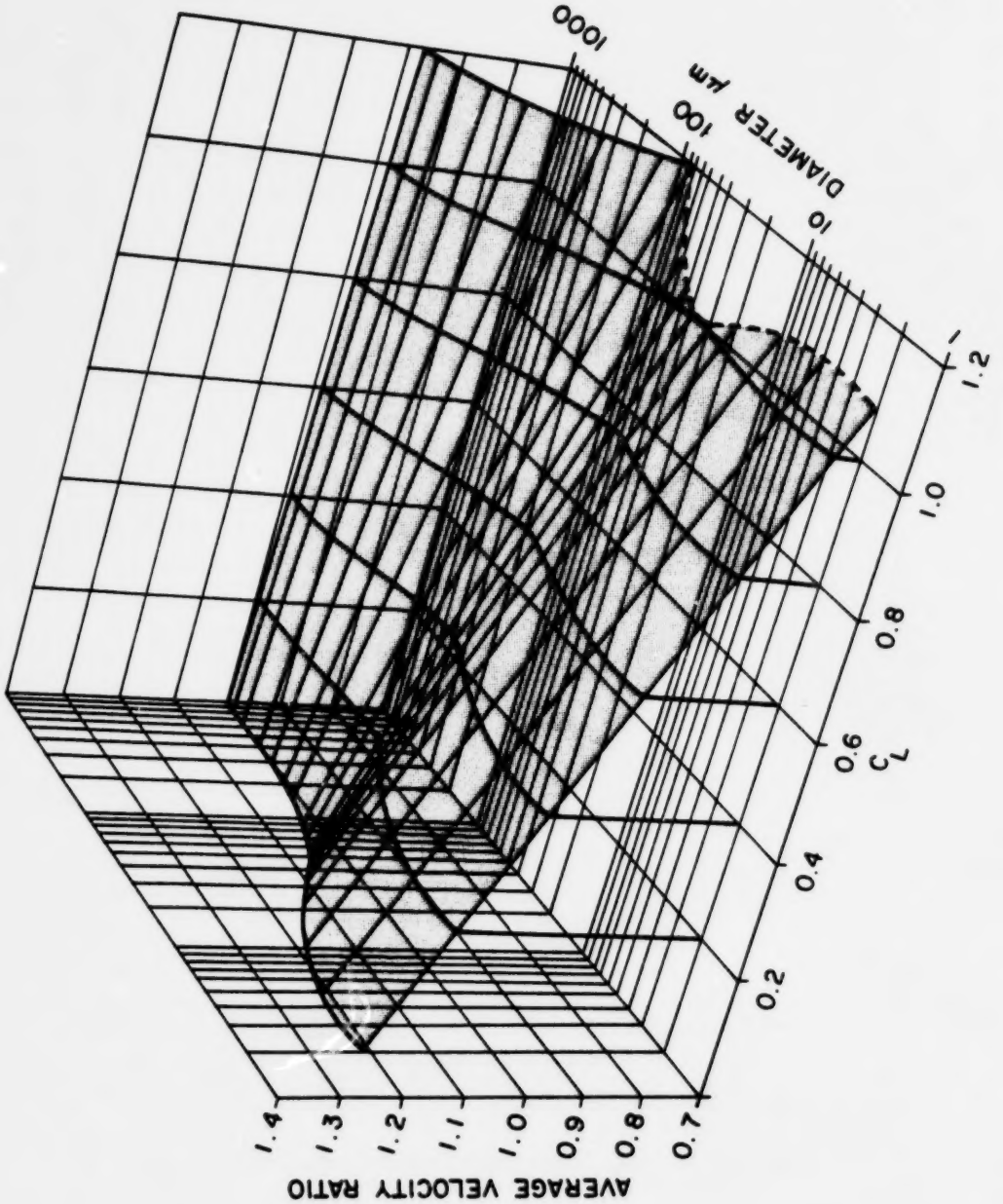

FIG. 9: DROP VELOCITY

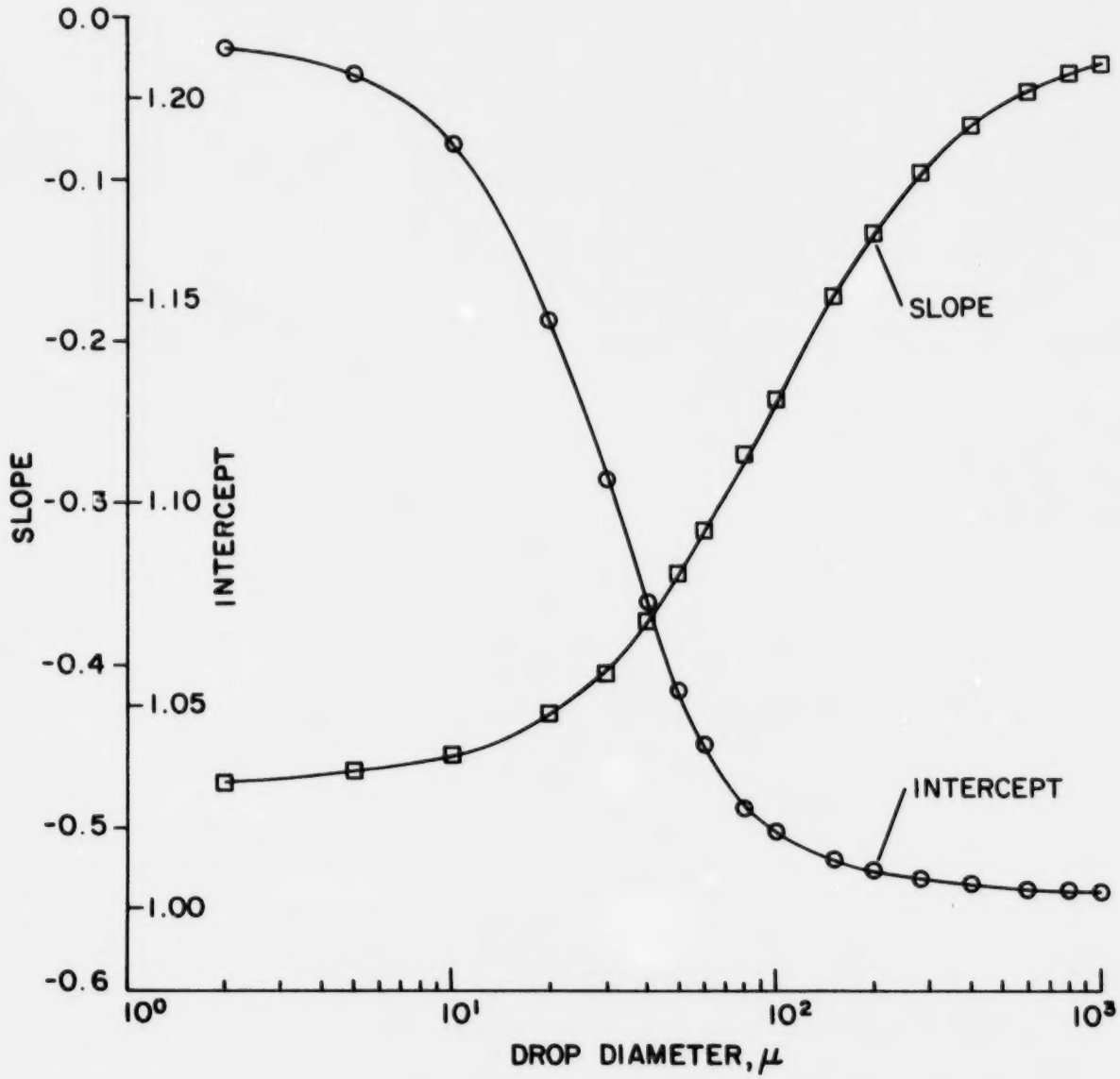

FIG. 10: VELOCITY RATIO PARAMETERS

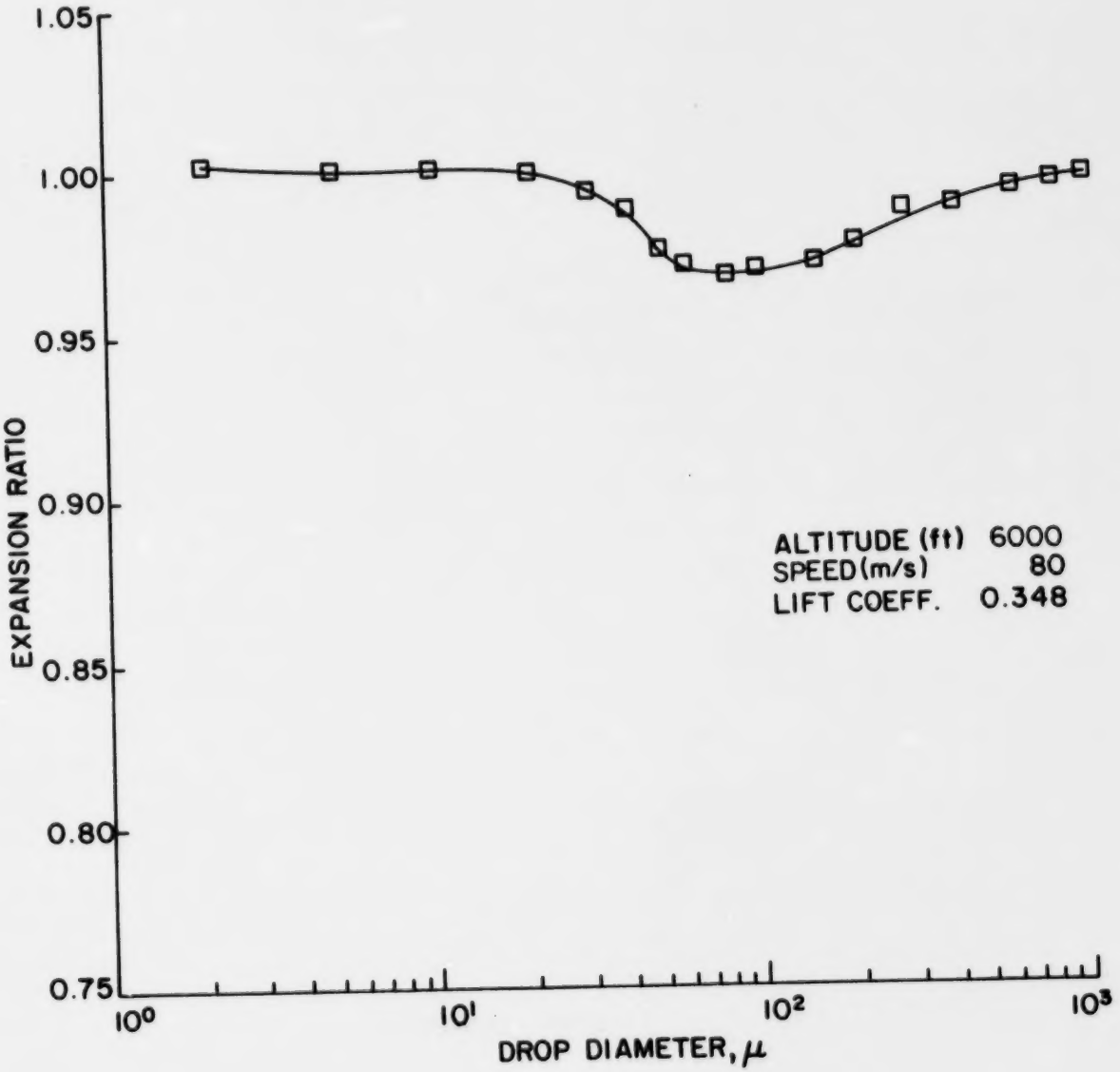

FIG. 11: TRAJECTORY EXPANSION

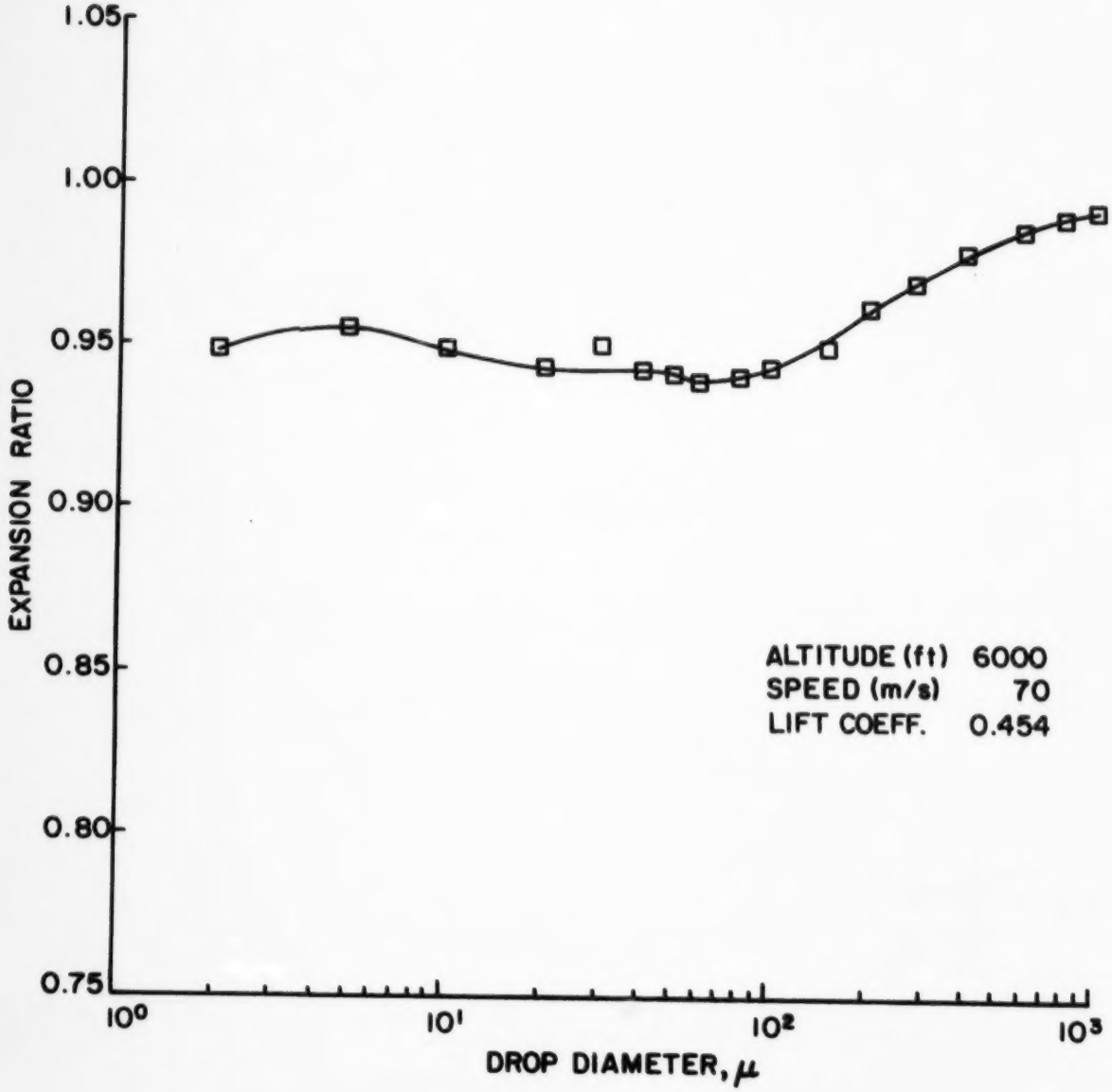

FIG. 12: TRAJECTORY EXPANSION

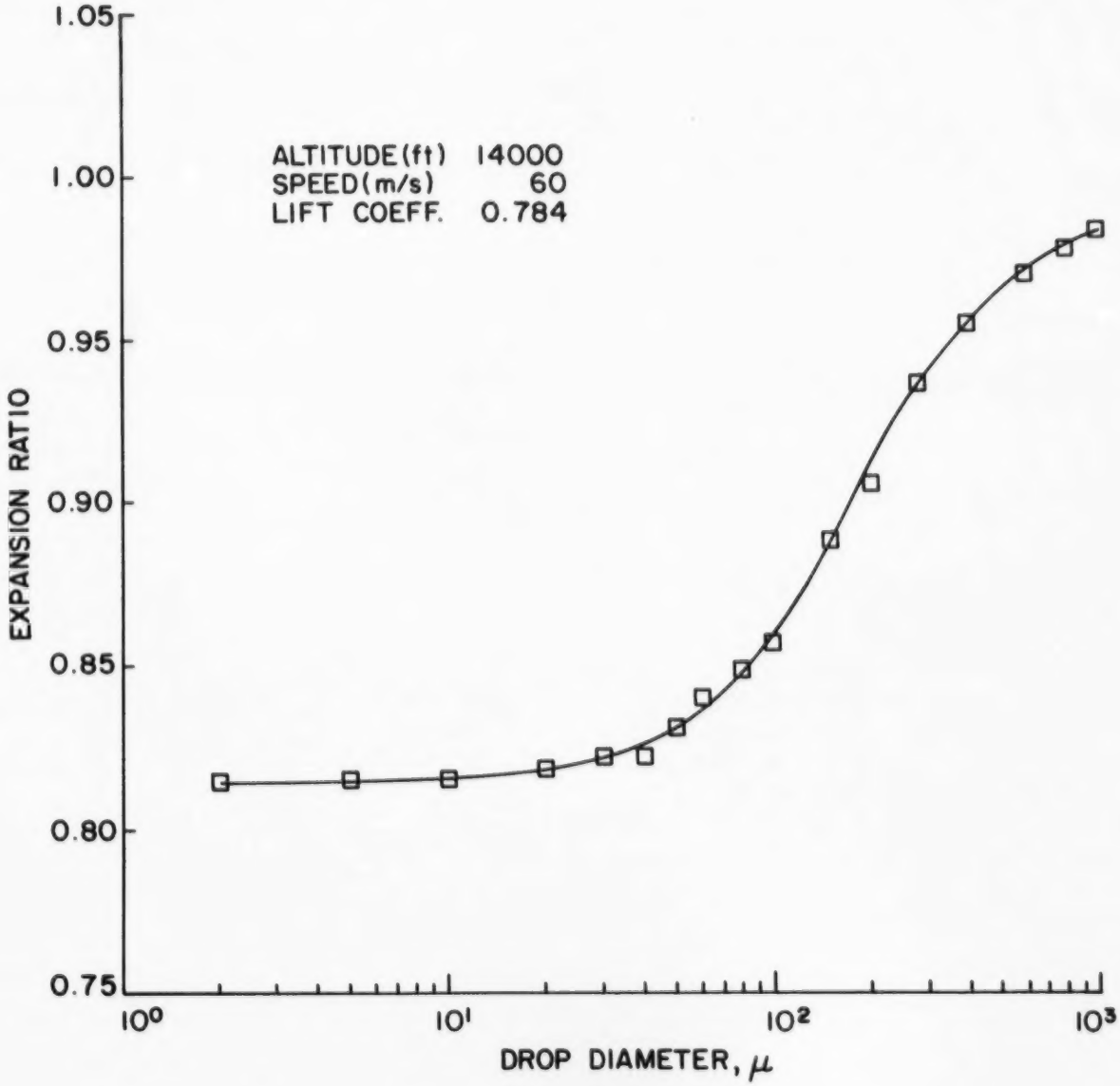

FIG. 13: TRAJECTORY EXPANSION

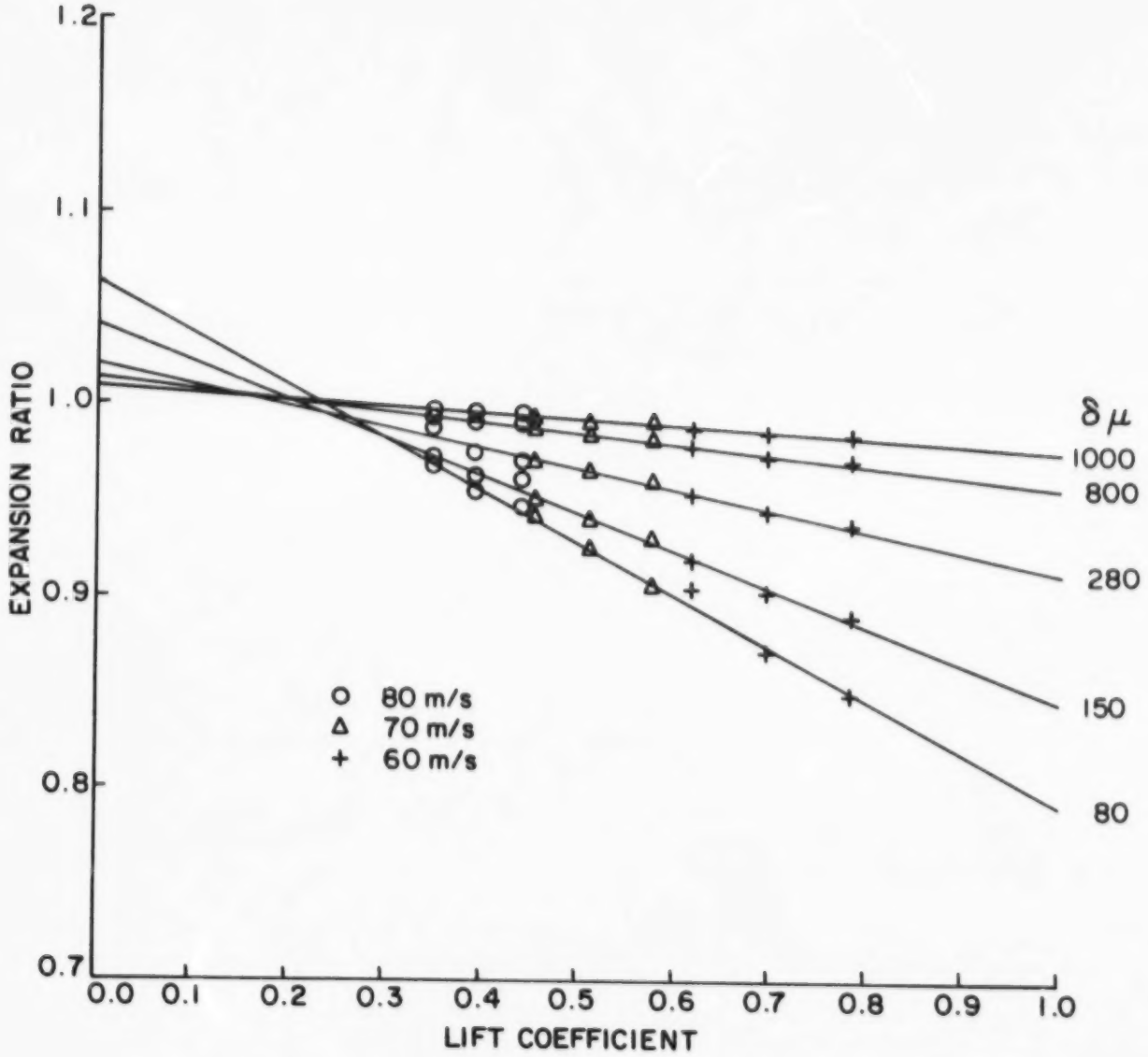

FIG. 14: TRAJECTORY EXPANSION

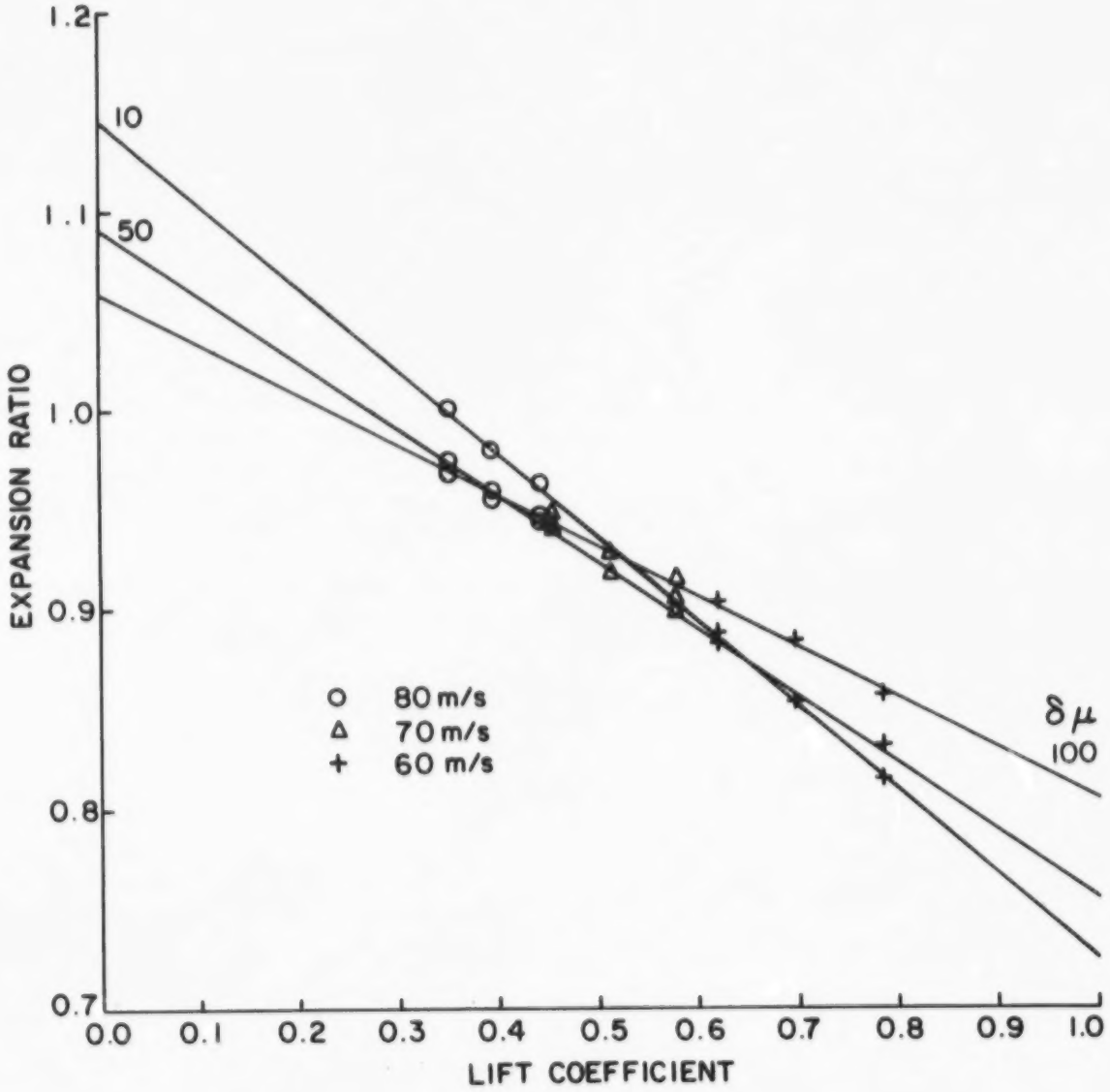

FIG. 15: TRAJECTORY EXPANSION

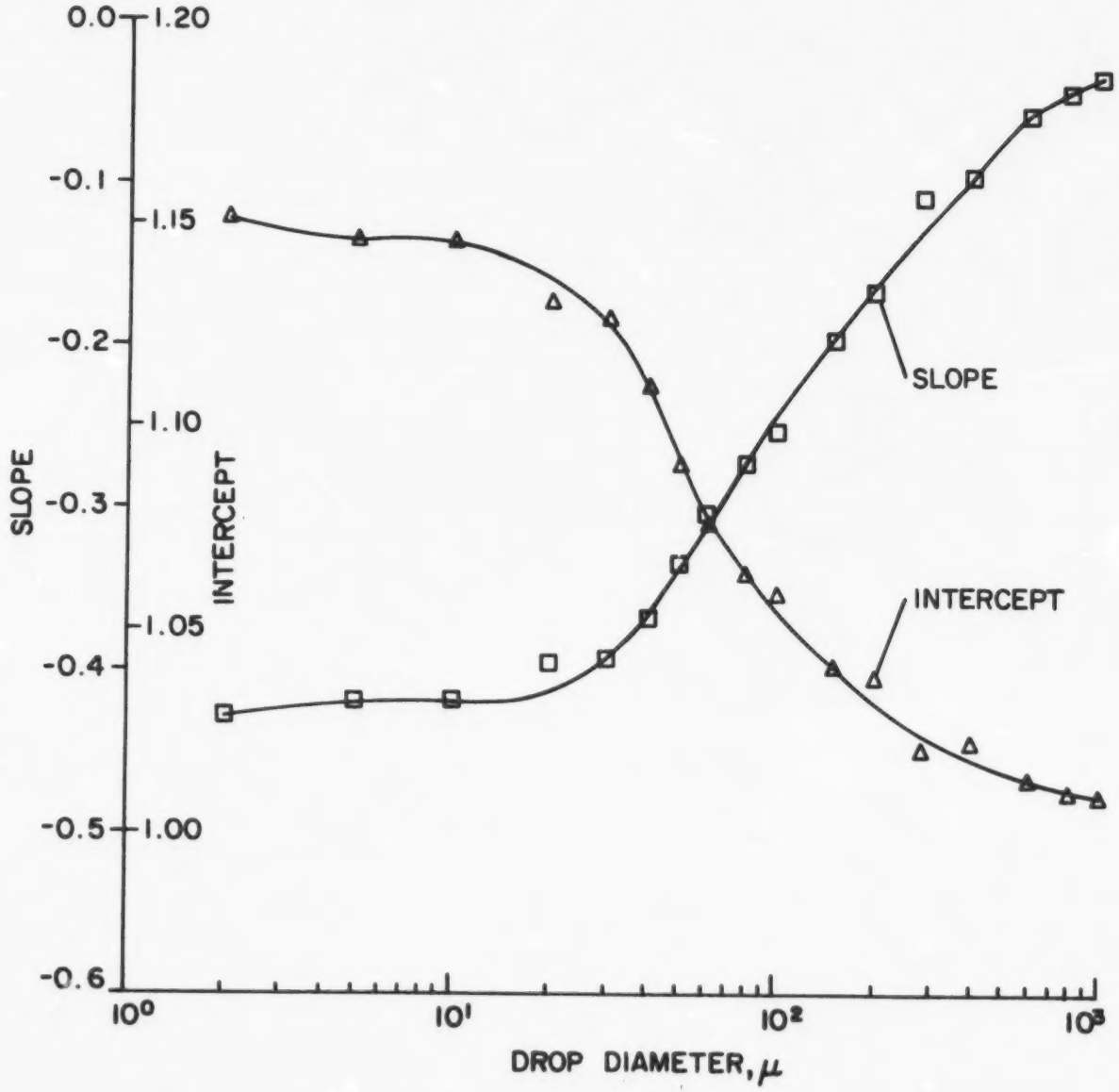

FIG. 16: EXPANSION RATIO PARAMETERS

REPORT DOCUMENTATION PAGE / PAGE DE DOCUMENTATION DE RAPPORT

REPORT/RAPPORT NAE-AN-21 1a	REPORT/RAPPORT NRC No. 23508 1b
REPORT SECURITY CLASSIFICATION CLASSIFICATION DE SÉCURITÉ DE RAPPORT Unclassified 2	DISTRIBUTION (LIMITATIONS) Unlimited 3

TITLE/SUBTITLE/TITRE/SOUS-TITRE

Aircraft Flow Effects on Cloud Droplet Images and Concentrations

4

AUTHOR(S)/AUTEUR(S)

A.M. Drummond

5

SERIES/SÉRIE

Aeronautical Note

6

CORPORATE AUTHOR/PERFORMING AGENCY/AUTEUR D'ENTREPRISE/AGENCE D'EXÉCUTION

National Research Council Canada
National Aeronautical Establishment — Flight Research Laboratory

7

SPONSORING AGENCY/AGENCE DE SUBVENTION

8

DATE	FILE/DOSSIER	LAB. ORDER COMMANDE DU LAB.	PAGES	FIGS/DIAGRAMMES
84-06			37	16
9	10	11	12a	12b

NOTES

13

DESCRIPTORS (KEY WORDS)/MOTS-CLÉS

1. Clouds — measurement
2. Drops — measurement
3. Cloud physics

14

SUMMARY/SOMMAIRE

Cloud physics measurements by the Twin Otter aircraft are affected to some degree by local flow effects from the wing and from the probe canister. Droplet images and concentration are distorted in the worst case by no more than 20% for an aircraft lift coefficient (C_L) of 0.75 and by only a few percent for low values of C_L. Corrections for a Particle Measuring Systems probe mounted on a short pylon at the inboard spanwise location have been given which are based on an experimentally verified model for the flow velocity.

15